Time−Temperature and Time−Concentration Superposition of Nanofilled Elastomers: A Molecular Dynamics Study

Jun Liu,[†,‡] Dapeng Cao,[*,‡] Liqun Zhang,[*,†] and Wenchuan Wang[‡]

Key Laboratory of Beijing City on Preparation and Processing of Novel Polymer Materials, and Division of Molecular and Materials Simulation, Key Laboratory for Nanomaterials, Ministry of Education, Beijing University of Chemical Technology, Beijing 100029, P. R. China

Received December 9, 2008; Revised Manuscript Received February 19, 2009

ABSTRACT: We systematically investigated the structural and dynamic properties of nanofilled elastomer on the basis of the idealized model of elastomer and nanoparticle. The simulated results indicate that the introduced nanoparticles induce more efficient chain packing. Meanwhile, a mobility gradient of polymer chains is found to exist approaching the nanoparticles. For the dynamic properties, we find for the first time that both the time−concentration and time−temperature superposition principles (TCSP and TTSP) are applicable at the chain length scale, while both break down at the segmental length scale for the filled system. However, the TTSP still holds at the segmental length scale for the pure system. Furthermore, the time−temperature−concentration superposition principle (TTCSP) applies well for the terminal relaxation of polymer nanocomposites. This scaling behavior has the underlying implication that the rheological properties (i.e., steady-state shear viscosity) of polymer nanocomposites possess thermorheological simplicity. In addition, interestingly, the characteristic relaxation time as a function of filler concentration exhibits an Arrhenius temperature dependence, if the concentration variation is regarded as an inverse of temperature variation. We suggest the introduced nanoparticles exert the similar effect to the thermodynamic variables (e.g., pressure and temperature) on the polymer dynamics. Lastly the stress relaxation of the model system is also examined. The decay of the bond orientation of polymer chains during the relaxation process is studied by changing the draw ratio, the filler loadings and the affinity between the nanoparticle and polymer. In order to equivalently investigate the stress relxation, we propose a new approach named conformational relaxation. It is observed that the conformational relaxation can be approximately fitted well by an exponential function for the pure and filled systems, similar to the stress relaxation. The TTSP is also applicable for the conformational relaxation of the pure system, while breaks down for that of the filled system. The relaxation time extracted by fitting the conformational relaxation curves with an exponential function at different temperatures, exhibits an Arrhenius relationship with the temperature for the pure and filled systems. Moreover, contrary to the isotropic dynamics during the creep process of the polymer from the simulated results of de Pablo, our simulated result shows an anistropic polymer dynamics with an accelerated relxation in the predeformed direction during the stress relaxation process.

1. Introduction

The topic of polymer nanocomposites is of great interest since the incorporation of nanoparticles to polymers can yield novel materials with exceptional properties, such as mechanical and barrier properties. The insight into the relationships between the composition, structure and properties of polymer nanocomposites will facilitate the development of design rules to engineer materials with desired properties. Many researches have been devoted to studying the addition of nanoparticles into the polymer. However, many of the conclusions have not yet been reconciled. For instance, the viewpoint about the effect of nanofiller on the chain conformation is not consistent yet, which has been addressed by different experimental and simulation approaches.[1−11] Additionally, another intriguing problem is that the glass transition of polymer nanocomposites has been reported to increase,[12,13] decrease,[14] or remain unaffected, in comparison with that of the pure polymer, and sometimes a second glass transition has as well been observed,[15] while presently no satisfactory model can reconcile these results in a reasonable way. As for the dynamics of the nanofilled polymer system, there are two dynamic processes reported experimentally for the adsorbed and nonadsorbed polymer segments.[16−19] In the case of C_{60}-polymer nanocomposites, by using several experimental techniques such as dynamic mechanical thermal analysis (DMTA) and incoherent neutron scattering Kropka et al.[20] found that the retarded polymer segmental mobility is attributed to the strong segments−C_{60} interactions, which ultimately suppress the overall polymer dynamics. In another paper, through incoherent elastic neutron scattering (IENS) they also pointed out that the impact of C_{60} on polymer dynamics is limited to the vicinity of the particles at nanosecond time scales.[21] For the nanofiller reinforced elastomer system, by using nuclear magnetic resonance (NMR) and performing mechanical measurements Montes et al.[22,23] observed the existence of a glass transition gradient in the vicinity of the particles, which suggests that particles are responsible for the nonlinear viscoelasticity behavior of the reinforced elastomer, attributed to strain-softening and melting of the glassy polymer shell surrounding the nanoparticle surfaces. Meanwhile, by using molecular dynamics simulation, Starr et al.[10] aslo found a mobility gradient of polymer chains approaching the nanoparticle surface in the case of nonattractive or attractive polymer/nanoparticle interaction. In contrast to these observations, recently experimental results from Roland et al.[24] indicate that the local segmental dynamics of the chains closely around the nanoparticles is indistinguishable from the motions of the bulk chains for the nanosized silica particles and poly(vinyl acetate) (PVAc) system. Interestingly, Mackay et al.[25,26] reported that the addition of the nanoscopic polystyrene(PS) nanoparticles to the linear PS

* Corresponding authors. E-mail: (D.C.) caodp@mail.buct.edu.cn; (L.Z.) zhanglq@mail.buct.edu.cn.

† Key Laboratory of Beijing City on Preparation and Processing of Novel Polymer Materials, Beijing University of Chemical Technology.

‡ Division of Molecular and Materials Simulation, Key Laboratory for Nanomaterials, Ministry of Education, Beijing University of Chemical Technology.

10.1021/ma802744e CCC: $40.75
Published on Web 03/09/2009

will lead to a dramatic viscosity reduction, which is contrary to the common observation that the addition of particles to liquids, even in polymeric liquids, produces an enhancement in viscosity, just as predicted by Einstein nearly a century ago. In line with the results from Mackay et al., Cosgrove et al.[27] also observed a surprising increase in chain mobility and a decrease in the shear viscosity related to the data for the pure polymer below a critical particle concentration for the high molecular weight poly(dimethylsiloxane)s blended with polysilicate nanoparticles.

It is noted that the investigation about the molecular origins of the reinforcement mechanisms of nanoparticles in polymer nanocomposites deserves our great attention, due to its broad range of applications. For instance, these carbon black and recently silica reinforced rubber materials have been widely used for many years, but they were not studied by considering as nanocomposites until now. Generally, there are two theories interpreting the reinforcement of rubber nanocomposites. An idea put forward previously suggests that reinforcement takes effect once the filler concentration is above the percolation threshold. This viewpoint is in contrast to the experimental observation that the filled polymers are reinforced once the good dispersion is achieved. In comparison with this standpoint, another theory is the transient filler network theory, which proposes that fillers are connected by a network of adsorbed chains forming a "second" (i.e., in addition to the entanglements) network. The latter was used satisfactorily by Sternstein et al.[28] to qualitatively explain the nonlinear viscoelastic properties such as the Payne effect observed in nanocomposites. At the same time, Kumar et al.[29,30] also adopted molecular dynamics simulations to address the mechanical reinforcement mechanism of polymer nanocomposites. More relevant reviews about the mechanism of the nanofiller reinforced elastomer can be found in these literatures.[31−34] It should be noted that for the filled elastomer system, Wang et al.[35] found that a single smooth master curve can not be obtained for viscoelastic properties of filled rubber systems when shifting along the frequency scale, which is mainly attributed to the polymer−filler interaction. This observation indicates the breakdown of the time−temperature superposition principle (TTSP) for filled elastomer systems.

Additionally, the stress relaxation of nanofilled elastomers is a very interesting topic, since it contains much knowledge about the fundamental polymer physics.[36] The advancement of the knowledge about the stress relaxation is a key to the engineering application of the rubber sealing rings.[37] Through the experimental methods, Madkour et al.[36,38] studied the filler effect on the stress relaxation of rubber vulcanizates in detail. By using the coarse-grained model, Weiner et al.[39−45] investigated systematically the stress relaxation of the model polymer melt. Harmandaris et al.[46] also explored the stress relaxation under the steady-state uniaxial elongational flow of the polyethylene (PE) melts by employing the atomistic model.

In general, according to all the issues mentioned above, the further investigation is needed to elucidate the complexity of polymer nanocomposites. An overview about the different aspects of polymer nanocomposites can be found in recently pulished reviews.[47,48] Currently, computer simulation and modeling are playing an increasing role in addressing the fundamental issues of polymer nanocomposites, in predicting and designing material properties and in guiding the experimental work like synthesis and characterization. In the present work, our main objective is to employ molecular dynamics simulation to study the nanofilled model elastomer system. Here we adopt the simplest model that can capture the essential features of a rubbery material at the atomic scale. The model elastomer is idealized as a collection of atoms which interact by two types of potentials. A bonding potential represents the covalent bonds that are responsible for the chains; and a potential describes the interactions between all nonbonded atoms including interchain and intrachain. In this work, the covalent bonds are represented by a finite extensible nonlinear elastic (FENE) potential, while the nonbonded interactions are approximated using a Lennard-Jones (LJ) potential. This idealized elastomer model is exactly the same as that from Weiner et al.[49,50] and our recent work.[51] For computation efficiency, here the interaction between the monomers of the model elastomer is purely repulsive.

The remainder of this paper is designed as follows. In section 2, we briefly describe our model and the needed simulation technique. Then, the results of these simulations are discussed in section 3, and some comparisons are made between the recent available experimental results and also some relevant simulations. Finally, the important conclusions are presented in section 4.

2. Models and Simulation Methods

The elastomer is represented by using a bead-spring model just as mentioned above. In our simulation, the idealized model elastomer consists of thirty beads with mass equal to unit. The total number of simulated polymer monomers is 6000. Although these chains are rather short, they already show the static and dynamic behavior characteristic of long chains in the polymer. Each bond in this model would correspond to $n = 3-6$ covalent bonds along the backbone of a realistic chemical chain when mapping the coarse-grained model to a real polymer. The truncated and shifted LJ potential for nonbonded interactions between all monomers is as follows:

$$U(r) = \begin{cases} 4\varepsilon\left[\left(\frac{\sigma}{r}\right)^{12} - \left(\frac{\sigma}{r}\right)^{6}\right] + C & r < 1.12\sigma \\ 0 & r \geq 1.12\sigma \end{cases} \quad (1)$$

Here C is equal to ε and the LJ interaction is cut off at the distance $r = 1.12\sigma$. Since it is not our aim to study a specific polymer, we use the LJ units where ε and σ are set to unit. It means that all calculated quantities are dimensionless. The interaction between the adjacent bonded monomers is represented by a stiff finite extensible nonlinear elastic (FENE) potential:

$$V_{\mathrm{FENE}} = -0.5kR_0^2 \ln\left[1 - \left(\frac{r}{R_0}\right)^2\right] \quad (2)$$

where $k = 30\varepsilon/\sigma^2$ and $R_0 = 1.5\ \sigma$, guaranteeing a certain stiffness of the bonds while avoiding high-frequency modes and chain crossing. The nanoparticles are modeled as Lennard-Jones spheres of radius R_n, which is equal to 2σ. The interactions between polymer segments and smooth nanoparticles, nanoparticles and nanoparticles are modeled using modified Lennard-Jones functions, which account for the excluded volume of the beads and particles by offsetting the interaction range by R_{EV} as follows:

$$U_{np}(r) = \begin{cases} 4\varepsilon_{np}\left[\left(\frac{\sigma}{r - R_{\mathrm{EV}}}\right)^{12} - \left(\frac{\sigma}{r - R_{\mathrm{EV}}}\right)^{6} + \frac{1}{4}\right] & r > R_{\mathrm{EV}} = R_n - \sigma/2 \\ \infty & r \leq R_{\mathrm{EV}} = R_n - \sigma/2 \end{cases} \quad (3a)$$

$$U_{nn}(r) = \begin{cases} 4\varepsilon_{nn}\left[\left(\frac{\sigma}{r - R_{EV}}\right)^{12} - \left(\frac{\sigma}{r - R_{EV}}\right)^{6} + \frac{1}{4}\right] & r > R_{EV} = 2R_n - \sigma \\ \infty & r \le R_{EV} = 2R_n - \sigma \end{cases} \quad (3b)$$

Here U_{np} and U_{nn} denote the polymer−nanoparticle and the nanoparticle−nanoparticle interactions, respectively. R_n is the radius of nanoparticle and r is the distance between interacting sites. The interaction parameter ε_{nn} is set as 1.0, while we change ε_{np} to represent the different interactions between the model elastomer and nanoparticles. Here we define $\varepsilon_{np} = 5.0$ as the "wet" interaction between the model elastomer and nanofiller, while $\varepsilon_{np} = 8.0$ as a "strong wet" interaction. In most cases the "wet" interaction between the model elastomer and nanoparticles is adopted. The monomer-particle interaction in the system is truncated and shifted at the separation $r = R_{EV} + 2.5\sigma$, while the interaction between particles is truncated and shifted at $r = R_{EV} + 2^{1/6}\sigma$. These models are all the same to those used in our previous paper.[52]

In our MD simulations, the *NVT* ensemble is adopted, where the temperature is fixed at $T^* = 1.0$ by using a Nose−Hoover thermostat, and the reduced number density of monomer is fixed at $\rho^* = 0.85$, which corresponds to that of a dense melt. Periodic boundary conditions are employed in all three directions. For the filled systems, the volume of the simulation box is increased so that the volume fraction of the polymers is the same as that of the neat systems. The velocity−Verlet[53] algorithm is used to integrate the equations of motion, with a time step $\delta t = 0.001$, where the time is reduced by τ. To generate the initial configurations, we place the polymer chains of stretching conformation in a large box, and obtain a system of low density. Then, the NPT simulation is used to compress the system of low density to the melt density. We equilibrate all structures over a long time so that each chain has moved at least $2R_g$. Such equilibrated structures are then used as starting configurations for production runs of $(10-20) \times 10^6$ MD steps, over which we collect structure and dynamics data for ensemble average. All MD runs are carried out by using the large scale atomic/molecular massively parallel simulator (LAMMPS), which is developed by Sandia National Laboratories.[54] Additionally this simulation software has as well been used to investigate the polyelectrolyte system.[55] More detailed descriptions can be found in the literature.[52]

3. Results and Discussion

3.1. Structure Properties. First, we focus our attention on the effect of the introduced nanofillers on the conformation of the polymer chains and the interchain packing, which may be altered by the filler-monomer interaction. We calculate the intra- and intermolecular radial distribution functions (RDFs). The structural properties are characterized by the intra- and intermolecular RDFs, namely $g_{intra}(r)$ and $g_{inter}(r)$ in Figure 1a,b. Here the monomer/nanoparticle interaction is "wet", and the number of nanoparticles is 24 and 48, respectively, corresponding to the filler volume fraction equal to 10.2% and 18.5%. For comparison, the calculated results of the pure system are also added to the figures. It can be observed from Figure 1 that the incorporation of nanoparticles has a negligible effect on $g_{intra}(r)$, which also indirectly indicates that the chain size is nearly independent of the addition of the particles. For $g_{inter}(r)$, with the increase of the filler loadings, the first and second peaks increase, though not obviously, implying the formation of a tighter chain packing due to the filler/monomer interaction. The simulated results also show that the density profile of the monomers around the particle exhibits pronounced oscillations with the increase of the particle volume fraction, as shown in Figure 2. In addition, chain end density and bond orientation of the polymer chains around the nanoparticles are also calculated (not shown here). The results show that the chain ends tend to aggregate near the particles, and the polymer segments around the particle align parallel to the particle surface. These results are in line with other simulations that have verified the tendency of chain segments to align parallel to the surface for both wall[56,57] and spherical nanoparticles.[8,10,58] Definitely, this simulated result is also supported by the experimental conclusion that a flattening of Poly(dimethylsiloxane) chains on the friction substrate surface was found.[59] All these evidence give us an emphasis that the behavior of the model used in this paper is consistent with that obtained from other different models used in the literature for investigation of nanocomposites. Furthermore, we also calculate the static structure factor of the pure and filled nanocomposites, which is obtained through the Fourier transform of the total pair distribution function, $g_{tot}(r)$, given by

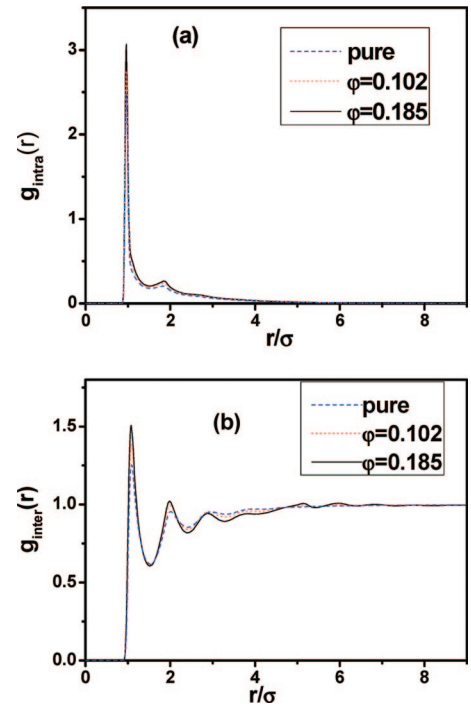

Figure 1. (a) Intramolecular pair distribution function for the pure and nanofilled systems with the "wet" interaction, obtained from the present MD simulations for chain length $N = 30$. (b) Intermolecular pair distribution function for the pure and nanofilled systems.

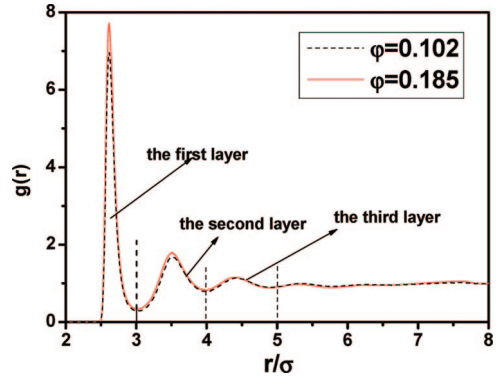

Figure 2. The nanoparticle-monomer pair distribution function for the filled system with the nanoparticle volume fraction $\varphi = 0.102$ and 0.185 for the "wet" interaction. The dash lines in the figure define several layers around the nanoparticle.

$$S(q) = 1 + \rho \int_0^\infty 4\pi r^2 \frac{\sin(qr)}{qr}[g_{tot}(r) - 1]\,dr \qquad (4)$$

Here ρ denotes the number density of the system and q is the momentum transfer. $S(q)$ vs q plots for the pure and filled system are presented in Figure 3. The figure demonstrates that the location of the first peak is around $q = 6.9$, and its intensity increases slightly with the increase of the nanoparticle concentration, which suggests a more efficient monomer packing. This point agrees well with the result from Figure 1b. In order to characterize the dispersion state of nanoparticles in the polymer matrix, the nanoparticle-nanoparticle density distribution function is also presented in Figure 4 for different number of particles with $N_n = 8$, 16, 24, and 48, corresponding to the filler volume fraction φ = 0.037, 0.074, 0.102, and 0.185 respectively. Clearly, the diameter of the model particle is 4σ. Figure 4 show that a strong peak appears at approximately $r = 5\sigma$ and a small peak at $r = 6\sigma$, which is a signal of "bridging cluster" of nanoparticles via one or two monolayers of the polymer. And these effects are strengthened with the increase in particle concentration. However, for all cases the direct aggregation of particles does not happen, just as evidenced by no peak at the location of $r = 4\sigma$. These observations are similar to the findings from the literature.[30,60]

For the nanofilled elastomer, the "bound rubber" is always referred to those polymer chains that are tightly adsorbed on the particle surface. Here we also calculate the first layer content of polymer segments, which is defined as the ratio of the number of those monomers within a distance of σ from the nanoparticle surface to the total polymer content. This is illustrated in the density profile of the monomers around the particle in Figure 2. The calculated result is plotted in Figure 5. The figure presents that the first layer content increases linearly with the filler loadings, attributed to more surface area of the introduced particles. In order to examine the monomer dynamics in the vicinity of the nanoparticles, for the case of the filled elastomer system with $N_n = 24$ we track the trajectory of a chosen monomer located in the first layer (marked in Figure 2) region of the corresponding nanoparticle at the initial time for the "wet" and "strong wet" particle/monomer interactions, and calculate the distance S_{n-m} between the chosen monomer and the corresponding nanoparticle at equal time intervals, as shown in Figure 6. In the figure, the dash lines represent the layer boundary obtained according to Figure 2. In the case of "wet" interaction, we can notice that the monomer mobility is restricted in the first layer region in a short time, then the monomer moves to the second and third layer region far away from the particle, where the distance between the monomer and the particle is more fluctuated, indicating an enhanced dynamics. However, in the case of "strong wet" interaction, the monomer is basically confined in the first layer region in the range of time studied. These analyzed results indicate the following two points. First, there exists a polymer mobility gradient approaching the nanoparticle, which is in agreement with the simulated results from Starr et al.,[10] but it may be not reasonable enough to suggest a glasss transition gradient existing around the nanoparticle.[22] Second, the adsorption/desorption process exists between the nanofiller and the polymer chains, and this desorption process will be greatly hindered by the stronger attractive interaction between the nanoparticle and polymer. This is in good agreement with the simulated results from the literature.[61]

3.2. Dynamic Properties. In this section, we investigate the effect of the nanoparticles on the dynamics of the polymer chains. In order to extract the effect of the nanoparticle on the relaxation behavior, following the idea of Starr et al.[10] and also our previous paper[51] we compute a dynamic quantity, i.e., the

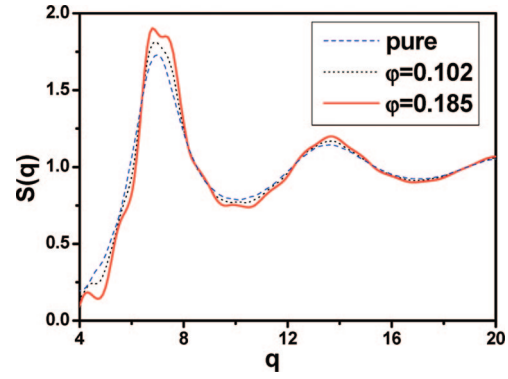

Figure 3. Static structure factor $S(q)$ for the pure and filled systems for the "wet" interaction. The location of the first peak corresponds to $q = 6.9\sigma$. The figure presents that the intensity of the first peak increases with the filler volume fraction increasing, indicating a much closer chain packing.

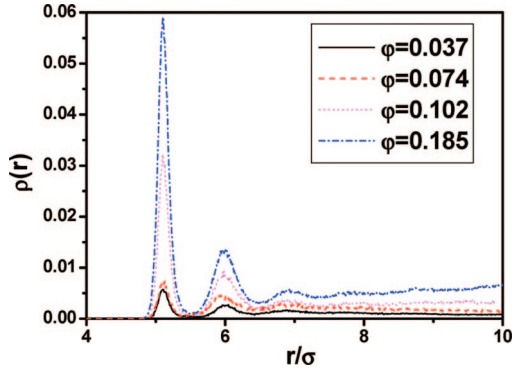

Figure 4. Nanoparticle−nanoparticle density distribution function for the different nanoparticle volume fractions.

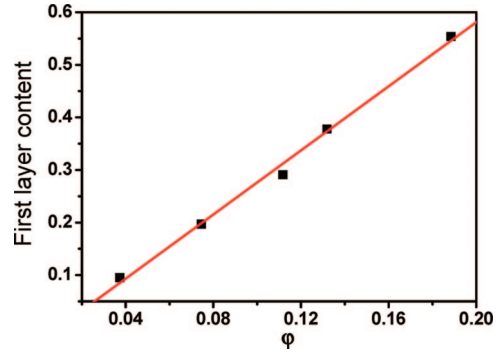

Figure 5. Plot of the first layer content with respect to the filler volume frcation. The figure suggests that the first layer content increases linearly with the filler concentration.

incoherent intermediate dynamic structure (IIDS) factor $\phi_q^s(t)$, by the relationship

$$\varphi_q^s(t) = \frac{1}{M}\sum_{m=1}^{M}\langle \exp(\mathbf{iq}\cdot[\mathbf{r}_m(t) - \mathbf{r}_m(0)])\rangle = \frac{1}{M}\sum_{m=1}^{M}\left\langle \frac{\sin(q\Delta r_m(t))}{q\Delta r_m(t)}\right\rangle \qquad (5)$$

where M stands for the total number of monomers in the polymer, $(\mathbf{r}_m(t) - \mathbf{r}_m(0))$ and $\Delta r_m(t)$ is the displacement of scattering center "m" after time t; q is the momentum transfer describing the spatial scale of the measurement, and the sum covers over all scattering centers. In addition, at the chain length

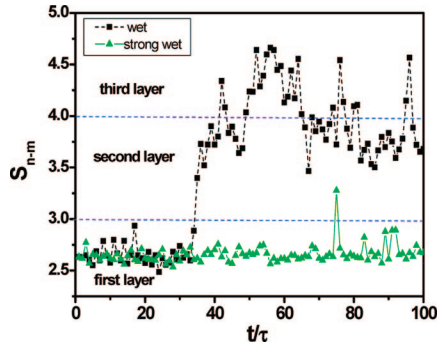

Figure 6. Trajectory of a chosen monomer located in the first layer region of the nanoparticle at initial time for the "wet" and "strong wet" interactions between the monomer-nanoparticle interaction. S_{n-m} represents the distance between the chosen monomer and the corresponding nanoparticle. Notedly $S_{n-m}$is calculated at equal time intervals. The result indicates a mobility gradient approaching the nanoparticle. τ is referred to the unit time of the simulation.

scale the terminal relaxation (the longest normal mode) in the simulated system can be evaluated through the time decay of the autocorrelation function for the chain end-to-end vector autocorrelation $\langle u(t)\cdot u(0)\rangle$, denoted by $\phi_{ete}(t)$ for different particle loadings. In parts a and b of Figure 7, we present the IIDS factor $\phi_q^s(t)$ at the first peak position of the static structure factor ($q = 6.9$ presented in Figure 3) and $\phi_{ete}(t)$ for different filler concentrations, which probe the dynamics at the segmental and chain length scales respectively. It can be found from the figures that the decay of $\phi_q^s(t)$ becomes much slower with the nanoparticle volume fraction increasing, implying a more retarded dynamics due to the chain segment and particle interaction. At the chain length scale a more restricted mobility is also observed with the particle concentration increasing. We define the characteristic relaxation times as τ_q^s at segmental length scale and τ_{ete} at chain length scale when the value of $\phi_q^s(t)$ and $\phi_{ete}(t)$ decays to 1/e respectively. In order to test the equivalence of the effect of the nanoparticles on the polymer dynamics, here we plot in parts c and d of Figure 7 $\phi_q^s(t)$ and $\phi_{ete}(t)$ for different nanoparticle loadings by rescaling the time with respect to the corresponding characteristic relaxation time.

Remarkably, by rescaling the time with respect to the corresponding characteristic relaxation time, at the chain length scale a globally universal curve of the end-to-end vector autocorrelation $\phi_{ete}(t)$is obtained for different particle loadings, as shown in Figure 7d, while at the segmental length scale we do not observe a universal master curve for the IIDS factor as shown in Figure 7c. These findings just indicate that the time−concentration superposition principle (TCSP) is applicable at the chain length scale, while the TCSP breaks down at the segmental length scale. We will present the physical interpretations later. In order to quantify the effect of the filler loadings on the dynamics of the polymer chains, we plot the characteristic relaxation time τ_q^s and τ_{ete} as a function of the nanoparticle concentration φ in Figure 8. The figure indicates that the dependence of the logarithm of the characteristic relaxation time of the end-to-end vector autocorrelation and IIDS factor on the particle concentration is approximately linear, and can be fitted well by the following relations:

$$\log(\tau_{ete}) = 6.24 + 8.98\phi$$
$$\log(\tau_q^s) = -1.02 + 2.91\phi \quad (6)$$

In fact, the relation in eq 6 can be considered analogous to the Arrhenius temperature dependence, if the nanoparticle concentration is regarded as an inverse of the temperature. This result suggests that the incorporation of the "wet" nanoparticles has the similar effect with the thermodynamic variables (such as the pressure) on the polymer dynamics.[62] Additionally, we also calculate the self-diffusion coefficient of the polymer chains, represented by D, as a function of the filler volume fraction. For calculation convenience, the quantity $6D$, figured out directly from the mean-square displacement according to the Einstein equation, is employed to represent the diffusion rate. This result is plotted in Figure 9, where the diffusion coefficient of the chains scales linearly with respect to the particle concentration, which is in fairly good agreement with the experimental results for poly(dimethylsiloxane) (PDMS) blended with silicate nanoparticles.[17]

Next, in the nanofilled elastomer system, we also examine the temperature effect on the dynamics of the polymer nanocomposites at the filler volume fraction $\varphi = 0.102$ and the "wet" particle/polymer interaction. At the segmental length scale, we calculate the incoherent intermediate dynamic structure (IIDS) factor $\phi_q^s(t)$, as shown in Figure 10a. The pure system is also added to the figure for comparison. The simulated results show that the decay of $\phi_q^s(t)$ for the pure and filled systems becomes much quicker with the temperature increasing. Moreover, at each temperature the decay of $\phi_q^s(t)$ for the filled system is slower than that of the pure system, but the difference becomes negligible with the temperature increasing, indicating that more chains adsorbed on the particle surface desorbed at high temperature. This can be understood by the fact that at low temperature the enthalpic contribution dominates due to the monomer/particle attraction, while at high temperature the entropic contribution comes into effect, and more chains leave the particle surface and become free. This is in line with the experimental observation that the amount of bound rubber is relevant to the temperature at which the extraction is performed.[63] This result is aslo similar to the simulated result from Starr et al.[10] Meanwhile, it is noted that the difference of the decay of $\phi_q^s(t)$ for the pure and filled systems becomes gradually more obvious at a long time for each temperature, as illustrated in Figure 10a. Additionally, we also calculate the end-to-end vector autocorrelation $\phi_{ete}(t)$ at different temperatures, i.e. the characteristic relaxation time at the chain length scale, shown in Figure 10b. Similar to the decay of $\phi_q^s(t)$, $\phi_{ete}(t)$ also decays more quickly with the temperature increasing.

Similarly, by rescaling the time with respect to the corresponding characteristic relaxation time, for the pure system a universal master curve is obtained at different temperatures, as presented in Figure 11a, indicating the time−temperature superposition principle (TTSP) is valid at the segmental length scale for the pure system, while breaks down for the filled system, as illustrated in Figure 11b. However, interestingly, at the chain length scale, the TTSP becomes applicable for the filled system evidenced by Figure 11c. In order to present a systematic study, we also plot the end-to-end vector autocorrelation $\phi_{ete}(t)$ for several systems at different nanoparticle concentrations and different temperatures, namely, $\varphi = 0.037$ and $T = 3.0$; $\varphi = 0.074$ and $T = 2.5$; $\varphi = 0.102$ and $T = 2.0$; $\varphi = 0.185$ and $T = 1.5$; $\varphi = 0.233$ and $T = 1.0$, and the simulated result is shown in Figure 10c. By rescaling the time with respect to the corresponding characteristic relaxation time, all curves are shifted to a single master curve just as shown in Figure 11d, suggesting the validity of the time−temperature-concentration superposition principle (TTCSP) at chain length scale.

After a thoroughly presenting the simulated results, here we can generalize the important conclusions obtained above. By calculating the two quantities $\phi_q^s(t)$ and $\phi_{ete}(t)$ over a relative broad range of temperatures and filler concentrations, both time−concentration superposition principle (TCSP) and time−temperature superposition principle (TTSP) break down at the

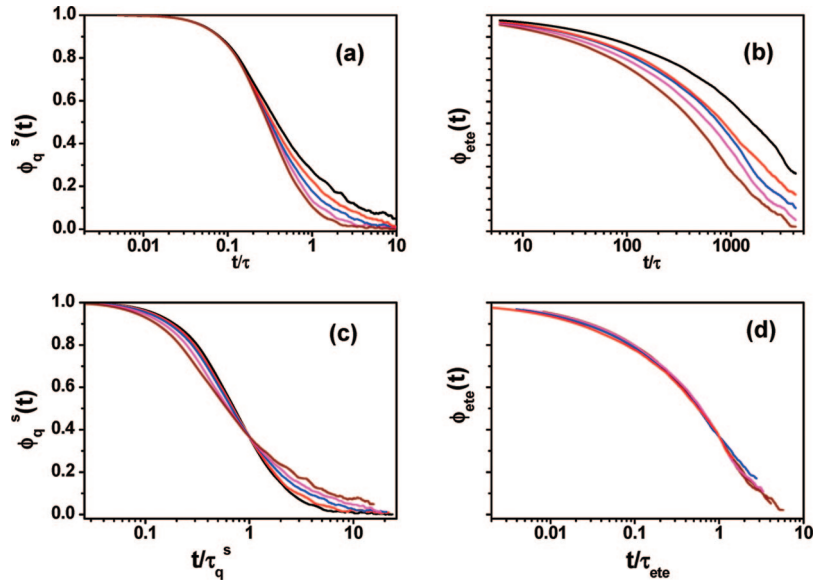

Figure 7. (a) Incoherent intermediate dynamic structure factor $\phi_q^s(t)$ and (b) the end-to-end vector autocorrelation $\phi_{ete}(t)$ for the filled system with different filler volume fractions $\varphi = 0.037$, 0.074, 0.102, 0.132 and 0.185. (c) Incoherent intermediate dynamic structure factor $\phi_q^s(t)$ and (d) the end-to-end vector autocorrelation $\phi_{ete}(t)$versus the rescaled time with respect to the corresponding characteristic relaxation time. τ is referred to the unit time of the simulation.

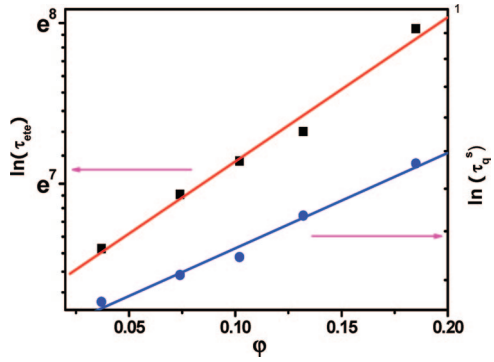

Figure 8. Logarithm of the characteristic relaxation time of $\phi_q^s(t)$ and $\phi_{ete}(t)$ versus the nanoparticle volume fraction. The result indicates an Arrhenius-like relationship between the characteristic relaxation time and the introduced filler concentration.

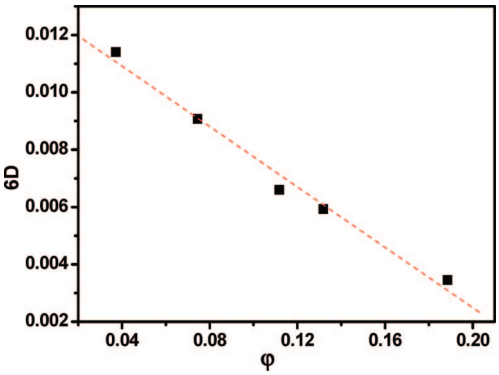

Figure 9. Diffusion coefficient of the polymer chains (D) with respect to the filler volume fraction. The figure indicates a good linear relationship between the diffusion coefficient and the filler loadings. This is consistent with the result from ref 17.

segmental length scale, while they become applicable at the chain length scale for the filled system. Notedly, the TTSP is applicable both at the segmental and chain length scales for the pure system. We can interpret these findings as follows. It is noted that the dynamics of the polymer segments are inhomogeneously retarded by the nanoparticles, because some

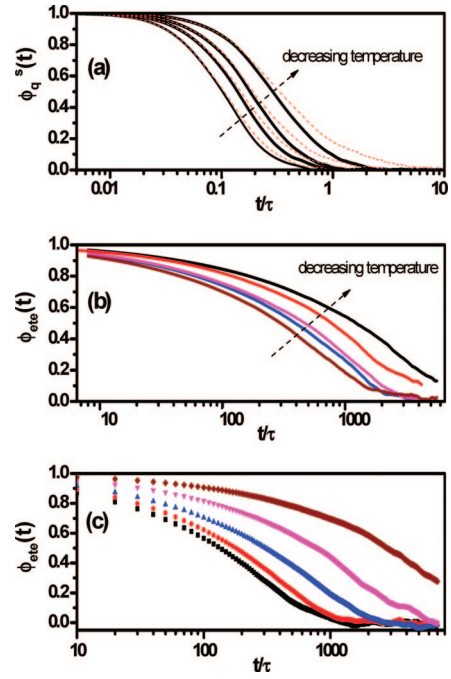

Figure 10. (a) Incoherent intermediate dynamic structure factor $\phi_q^s(t)$ for the pure system and the filled system with $\varphi = 0.102$ at different temperatures $T = 1.0$, 2.0, 3.0, and 5.0, where the solid and the dash lines represent the pure and filled systems, respectively. (b) End-to-end vector autocorrelation $\phi_{ete}(t)$ for the filled system with $\varphi = 0.102$ at different temperatures $T = 0.8$, 1.0, 1.2, 1.5, and 2.0. (c)the end-to-end vector autocorrelation $\phi_{ete}(t)$ for the filled system with different filler concentrations at different temperatures. Key: (■) $\varphi = 0.037$ and $T = 3.0$; (●) $\varphi = 0.074$ and $T = 2.5$; (▲) $\varphi = 0.102$ and $T = 2.0$; (▼) $\varphi = 0.185$ and $T = 1.5$; (◆) $\varphi = 0.233$ and $T = 1.0$; τ is referred to the unit time of the simulation.

polymer segments are strictly restricted in the vicinity of the particle attributed to the filler/polymer interaction, while some polymer segments are far away from the particle and exhibit the bulk behavior. Therefore, the effect of the nanoparticles on the dynamics of the polymer segments is strengthened with the time evolution, when randomly choosing an initial time. This is attributed to the dynamics of more monomers to be influenced

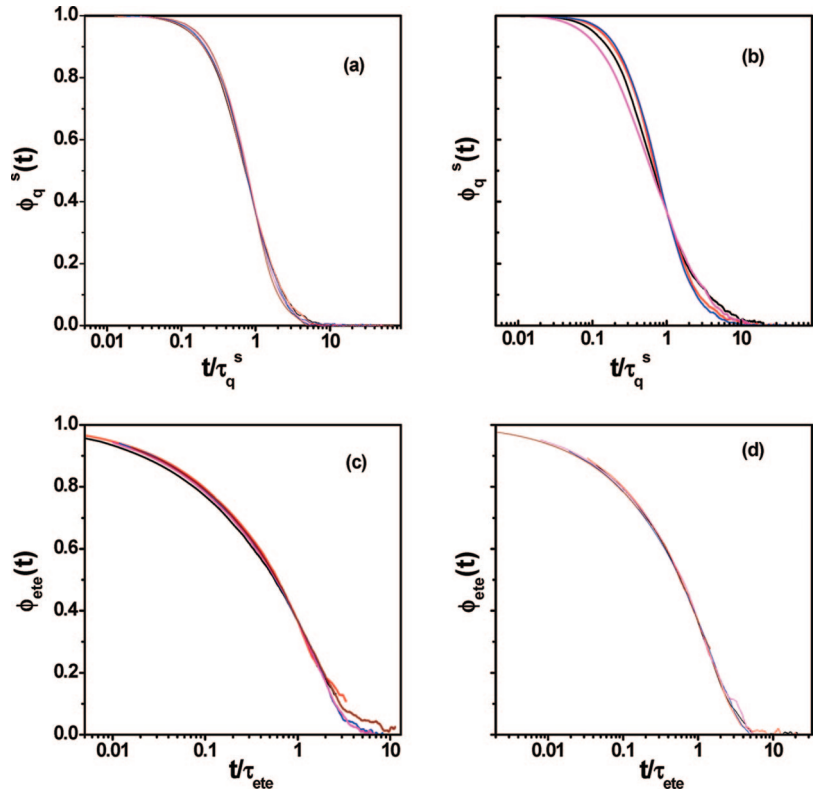

Figure 11. Incoherent intermediate dynamic structure factor $\phi_q^s(t)$for (a) the pure system at temperatures $T = 0.8$, 1.0, 1.5, 2.0, 3.0, and 5.0 and (b) the filled system with $\varphi = 0.102$ at temperatures $T = 1.0$, 2.0, 3.0, and 5.0 versus the rescaled time. (c) End-to-end vector autocorrelation $\phi_{ete}(t)$ for the filled system with $\varphi = 0.102$ at temperatures $T = 0.8$, 1.0, 1.2, 1.5, and 2.0 versus the rescaled time. (d) End-to-end vector autocorrelation $\phi_{ete}(t)$ for the filled system with different filler concentrations and at different temperatures with respect to the rescaled time.

by the nanoparticles, due to the adsorption/desorption process occurring in the nanoparticles and polymer interface.[61] This analyzed result as well rationalizes the big difference between the decays of $\phi_q^s(t)$ for the pure and filled systems at a long time in Figure 10a. This underlying reason also leads to the breakdown of the TTSP and TCSP at the segmental length scale for the filled system. However, at the chain length scale, we believe that the nanofillers exert homogeneously the same effect on all the polymer chains, which can be supported by the fact that nearly the same amount of the segments in every chain will be equally influenced by the addition of the nanoparticles, whose size is comparable to the polymer chains, at the simulated filler loadings. Certainly, the TTSP and TCSP will take effect at the chain length scale for the filled system, which of course make TTCSP valid at the chain length scale for the terminal relaxation.

On the basis of the analysis, we can extract a generalization that a homogeneous effect on the dynamics of the polymer chains at any length scale is needed for the validity of the TTSP and TCSP at the corresponding length scale. This also echoes the time-pressure superposition principle(TPSP) of the pure polymer in our previous publication,[51] where it is found that the TPSP holds at the chain length scale, but breaks down at the segmental length scale, which is also attributed to the dynamic heterogeneity at the segmental length scale induced by the high pressure. Therefore, we again suggest that the introduced nanoparticles play the similar role as the thermodynamic variables, like pressure, on examining the polymer dynamics.

Further, according to our simulated results, we claim that polymer nanocomposites do not belong to thermorheologically simple materials for their viscoelastic properties, so the shifting of isothermal sections can not produce a single master curve. It is because not all relaxation processes contributing to its viscoelastic properties obey the time−temperature superposition principle. However, it is noted that according to the research work from Heymans,[64] for such case where each relaxation process individually obeys the TTSP, the construction of a single master curve is still not possible if several overlapping transitions with different temperature dependences are present. If so, it would be invalid to extend the time (or frequency) scale beyond the range that could normally be covered in a single experiment for the polymer nanocomposites. This analysis is just in good agreement with the experimental observation from Wang et al.[35]

We again point to the finding that the terminal relaxation can be consistently described well by the TTSP and TCSP, and also TTCSP. In principle, this scaling behavior for the terminal relaxation $\phi_{ete}(t)$ is reminiscent of an approach that can be employed to study the rheological properties of filled polymer system. According to the Rouse model, the zero-shear viscosity of the polymer melts scales linearly with the rouse time or the terminal relaxation time for a given temperature. According to our simulated results, it can be inferred that here the time−temperature-concentration superposition principle applies well for the steady-state shear viscosity, which characterizes the friction between polymer chains when they flow. Furthermore, in fact, this inferred conclusion has been observed in the polymer solutions that the excellent time−temperature superposition is obtained for the steady-state shear viscosity for fixed polymer molecular weight in both the linear and nonlinear regimes.[65] The universal single master curve is obtained by plotting the normalized viscosity as a function of the scaled shear rate by multiplying the corresponding terminal relaxation time. Apparently, the nonlinear behavior occurs when the shear rate exceeds the reciprocal of the terminal relaxation time. This conclusion is as well supposed to take effect for the pure polymer melts. But here we mainly emphasize both TTSP and TCSP will hold for the rheological properties of polymer

nanocomposites with good nanoparticle dispersion (the filler network is not included here). Physically, this suggests that the reduction of the viscosity, driven by an imposed steady-state shear rate, exhibits the equivalent result for the viscosity at a higher temperature, or for the case at a much lower filler concentration. Adopting this scaling principle will enable us to accurately obtain the viscosity at low shear rate, which is difficult to accurately measure at low shear rate in a single experiment of polymer nanocomposites. Moreover, for high filler loadings, it is also difficult to accurately measure the viscosity. Accordingly, we can equivalently measure the viscosity at a lower filler concentration at a lower temperature, and use the above scaling principle to obtain the one at high filler loadings. These implications will find great contributions in the application of processing for polymer nanocomposites.

3.3. Conformational Relaxation. In the above sections, we have studied the nanofilled system in the equilibrium state. Here, we intend to address the stress relaxation of the nanofilled elastomer in a nonequilibrium state, which is of great significance for the rubber sealing rings applications. We subject the simulation box to a constant-volume elongation at a constant elongation rate, $\dot{\varepsilon}$, in the z direction, using a constant-temperature MD algorithm. The interactions between atoms in the basic cell with image atoms across the cell wall serve to transmit the deformation to the atoms in the basic cell. We set the elongation strain-rate $\dot{\varepsilon} = 0.0327$, which is the same with the simulation work from Gao et al.[39] Then the relaxation is performed under *NVT* conditions. Obviously, it is a little difficult to extract the accurate stress by using molecular dynamics simulation, so we adopt a new approach in this work. It is known that during the relaxation process by fixing the tensile deformation, the elongated polymer chains will participate in the recoiling and rearrangement process, and also slip between each other, gaining a state with more chain conformations. This behavior mainly leads to the gradual decrease of the internal stress. On the basis of the analysis, we focus our attention on the conformational relaxation of the polymer chains rather than the stress after the deformation. Undoubtedly, it is equivalent to illustrate the relaxation process of the polymer nanocomposites by using these two approaches.

First, we calculate the changes in chain orientation due to the relaxation after the deformation at different draw ratios, where the orientation of chain segments is expressed in terms of second-order Legendre polynomials, $\langle P_2 \rangle$. This function describes the average of the θ angle between a given element (two adjoining monomers in the chain) and the reference direction, which in this work refers to the stretching direction. $\langle P_2 \rangle$, given by

$$\langle P_2 \rangle = (3\langle \cos^2 \theta \rangle - 1)/2 \tag{7}$$

whose possible values range from -0.5 to 1. $\langle P_2 \rangle = -0.5$ indicates a perfect orientation perpendicular to the reference direction, whereas $\langle P_2 \rangle = 1$ means a perfect alignment parallel to the reference direction. When the segments are randomly oriented, we get $\langle P_2 \rangle = 0$. The simulated result of the nanofilled system with $\varphi = 0.102$ is shown in Figure 12a. We can observe from the figure that the bond orientation increases with the tensile draw ratio increasing, evidenced by the value of $\langle P_2 \rangle$ at $t = 0$. During the relaxation, the bond orientation decreases gradually. In order to reasonably examine the influence of draw ratio λ on the decay of the bond orientation, following the approach introduced in the literature,[66] the normalized $\langle P_2 \rangle / \langle P_2 \rangle_{\text{initial}}$ values at different draw ratios as a function of time is presented in Figure 12b. According to this figure, it is obvious that values of $\langle P_2 \rangle / \langle P_2 \rangle_{\text{initial}}$ generally increase slightly with the draw ratio during any relaxation time, indicating that more

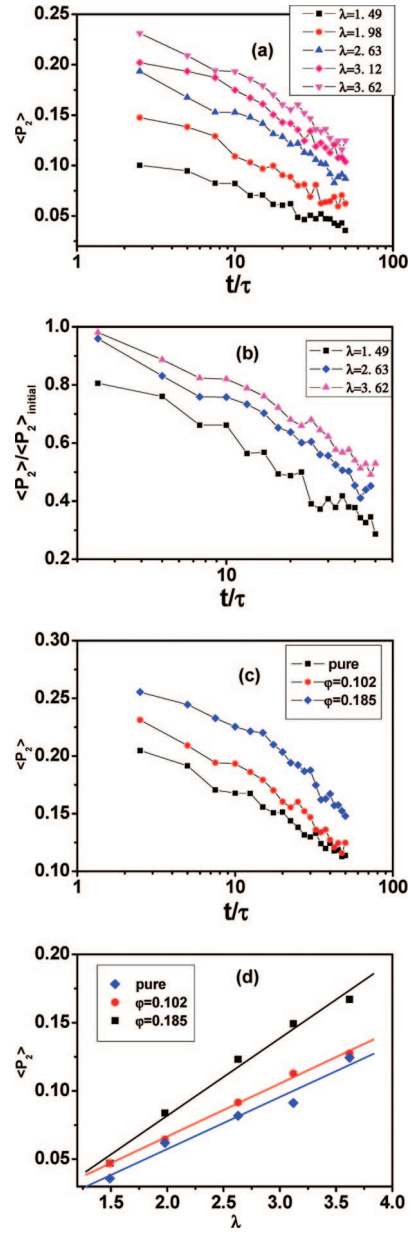

Figure 12. (a) Decay of the bond orientation $\langle P_2 \rangle$ at different draw ratios λ for the filled system with $\varphi = 0.102$. (b) Normalized values of $\langle P_2 \rangle / \langle P_2 \rangle_{\text{initial}}$ at different draw ratios λas a function of time. (c) Decay of the bond orientation at the draw ratio $\lambda = 3.62$ for the pure and filled systems with different filler loadings. (d) Value of $\langle P_2 \rangle$ at $t = 40\tau$ for the pure and filled systems as a function of the draw ratio λ. τ is referred to the unit time of the simulation.

oriented chains relax relatively slower. This also implies that the chains with stronger orientation need more time to recover the stability. These results are consistent with the atomistic modeling of poly(vinylphenol) from Brisson et al.[66] However, this finding is contrary to the fact that the driving force for relaxation is larger at higher draw ratios. But we suggest the relaxation rate is also related to other factors such as the mobility of polymer chains in the deformed direction. Additionally, in fact this observation is also supported by experimental studies of poly(ethylene terephthalate) (PET) relaxation behavior.[67] The underlying reason should be investigated further.

Meanwhile, we also plot in Figure 12c the decay of bond orientation at different filler volume fractions with the "wet" interaction between the filler and polymer. Here we observe that the rate of the decay of bond orientation is almost the same for the simulated particle loadings. But the bond orientation

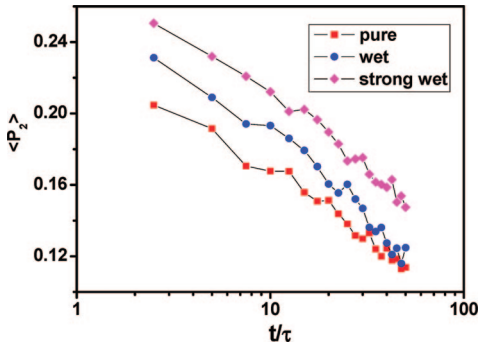

Figure 13. Decay of the bond orientation for the pure and filled systems with $\varphi = 0.102$ for the "wet" and "strong wet" polymer/nanoparticle interactions. τ is referred to the unit time of the simulation.

along the deformation direction increases at high filler loadings during tensile elongation, just according to the value of $\langle P_2 \rangle$ at $t = 0$. One possible interpretation to this result is that the chains can slip on the surface of the introduced nanoparticles, resulting in more ordered orientation during deformation, which may shed some light on the mechanical reinforcement for the polymer nanocomposites. Additionally, comparison of the chain orientation during relaxation at different draw ratios λ for different filler volume fractions is also shown in Figure 12d. The figure indicates that the values of $\langle P_2 \rangle$ at $t = 40\tau$ for the pure and filled systems increase linearly with the draw ratio. This result is in good agreement with the reported experimental data.[68] It can also be observed that the higher the filler loadings, the more ordered the bond orientation. For the different filler/polymer interactions, we also plot the decay of the bond orientation at initial draw ratio $\lambda = 3.62$ in Figure 13. The figure shows that the rate of the decay of bond orientation is approximatedly independent of the polymer/filler interaction in the simulated ranges.

Following this, we monitor the conformational relaxation, which can be characterized by

$$\delta R_{eed-z}(t) = \frac{R_{eed-z}(t) - R_{eed-z}}{R_{eed-z}} \tag{8}$$

where R_{eed-z} and $R_{eed-z}(t)$ stand for the root mean-square end-to-end distance in the z direction in the undeformed state and that at any time t during the relaxation, respectively. According to this definition, $\delta R_{eed-z}(t)$ will decay to zero at the final equilibrium state. The conformational relaxation for different filler loadings is shown in Figure 14a. Interestingly, it is found that the decay of $\delta R_{eed-z}(t)$ with respect to time for the pure system can be well fitted by an exponential function (the fitted curves are also presented in Figure 14a), which is similar to the stress relaxation function. This can be easily understood by the fact that the stress is directely proportional to the end-to-end distance for the nanofilled elastomer system.[4] However, for the filled systems with $\varphi = 0.102$ and 0.185, following the approach used in our previous paper,[51] the stretched exponential or Kohlrausch−Williams−Watts (KWW) function is adopted to more accurately fit these two curves, given by

$$\varphi(t) = \exp(-(t/\tau)^{\beta}) \tag{9}$$

By fitting these curves we get the corresponding relaxation time $\tau = 328.95$, 447.84, and 708.38 for the pure and filled systems of $\varphi = 0.102$ and 0.185 respectively. The result suggests that the conformational relaxation becomes much slower with the filler concentration increasing. Moreover, we also plot the decay of $\delta R_{eed-z}(t)$ for different filler/polymer interactions in Figure 14b. By fitting these curves we get the characteristic

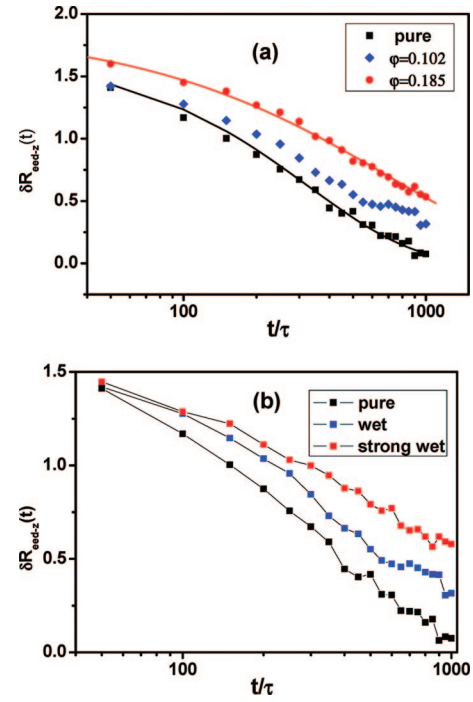

Figure 14. (a) Conformational relaxation for the pure and filled systems at different filler volume fractions in the case of "wet" interaction. (b) The conformational relaxation for the pure and filled systems for the "wet" and "strong wet" interactions with $\varphi = 0.102$. The figures show that the conformational relaxation can be well fitted by an exponential form, which is similar to the stress relaxation. τ is referred to the unit time of the simulation.

relaxation time $\tau = 328.95$, 447.84, and 649.35 for the pure, "wet", and "strong wet" interactions, respectively, which indicates a slower relaxation process for the strong interaction. We can explain these findings in terms of the increase of the activation energy, which influences the relaxation time:[38]

$$\tau = \tau_0 e^{\Delta U/RT} \tag{10}$$

The smaller the value of the activation energy ΔU and the higher the temperature, the smaller is the relaxation time and the faster is the conformational relaxation. The activation energy ΔU increases with the increases of the filler concentration and the filler/polymer interaction, which is attributed to the extra and stronger physical bonds formed between the chain segments and the filler surface, causing the increase of the viscosity of polymer nanocomposites. During the relaxation process, the nanoparticles retard the recoiling and rearrangement of the molecular chains, and this retardation extent increases at higher filler loadings and stronger polymer/filler interactions, evidenced by parts a and b of Figure 14. However, this effect exerted by the nanoparticles is not reflected when examing the decay of bond orientation, such as Figure 13.

It is well-known that the stress relaxation usually needs extremely long time far beyond the observation time, and the time−temperature superposition principle is usually adopted to solve this issue. Here we intend to test the application of the time−temperature superposition principle for the conformational relaxation of the pure and filled systems at the filler volume fraction $\varphi = 0.185$. The temperature effect on the conformational relaxation for the pure and filled systems is shown in parts a and b of Figure 15. We can observe from the figure that the conformational relaxation becomes much quicker at high temperature, attributed to the fact that more and more chain segments are able to get away from the nanoparticles and could, in fact, participate in the recoiling and rearrangement process.

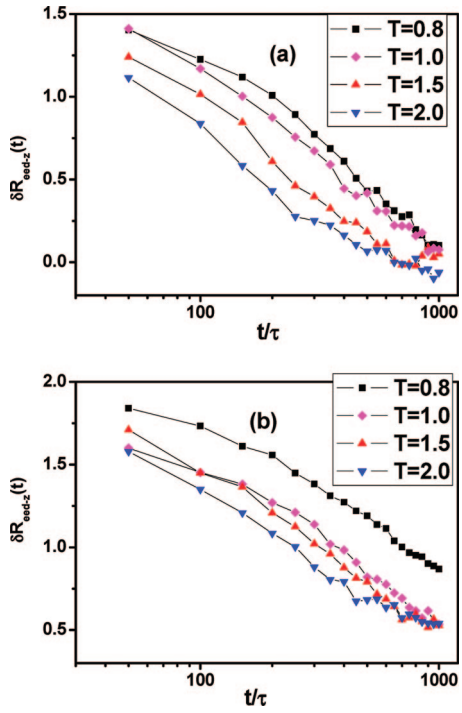

Figure 15. (a) Conformational relaxation for the pure system at different temperatures. (b) Conformational relaxation for the filled system with $\varphi = 0.185$ at different temperatures. τ is referred to the unit time of the simulation.

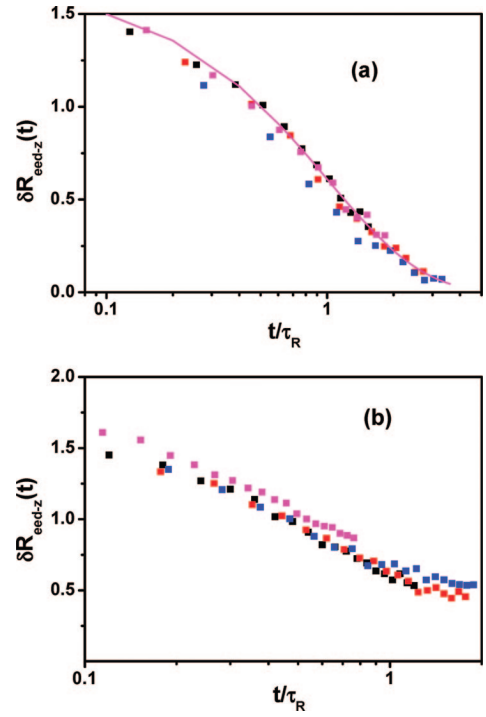

Figure 16. (a) Conformational relaxation versus the rescaled time with respect to the characteristic relaxation time for the pure system at different temperatures. (b) Conformational relaxation versus the rescaled time with respect to the characteristic relaxation time for the filled system with $\varphi = 0.185$ at different temperatures. The figures show that the time−temperature superposition principle (TTSP) is applicable for the pure system, while the TTSP breaks down for the filled system.

This can also be understood from eq 10. Furthermore, we use the exponential form to fit these curves in parts a and b of Figure 15 and obtain the corresponding relaxation time τ_R at each temperature. Similar to the case above, we plot in parts a and b of Figure 16 the conformational relaxations for the pure and filled systems by rescaling the time with respect to the corresponding relaxation time. It can be observed that all curves for different temperatures can be approximately reduced to a universal curve and be well fitted by an exponential function for the pure system, as shown in the Figure 16a, indicating the time−temperature superposition principle(TTSP) holds. However, for the filled system the curves can not be shifted to a single master curve (see Figure 16b), implying the TTSP is not applicable. This reason may be the same as the one mentioned above, i.e, the introduced particles exert a dynamic heterogeneity at the segmental length scale, which causes the temperature not to equivalently influence the relaxation of all chain segments, leading to the breakdown of the TTSP for the conformational relaxation. Finally, we plot the relaxation time with respect to the inverse of the temperature in Figure 17. The figure shows that the logarithm of the relaxation time scales linearly as a function of the inverse of the temperature, which is in good agreement with eq 10. However, according to the figure, the calculated activation energy ΔU is almost the same for the pure and filled systems at the temperatures simulated. This needs to be investigated in detail in the future.

In addition, we also examine the dynamics during the relaxation and test whether the dynamics is isotropic or not, because some reports indicate that the dynamics of the polymer during the creep process are enhanced isotropically in the three directions.[69] For the pure system we plot in Figure 18 the incoherent intermediate dynamic structure (IIDS) factor $\phi_q^s(t)$ at the segmental length scale in x, y, and z directions respectively. Interestingly, the figure exhibits an anisotropical acceleration of relaxation with a slightly enhanced dynamics in the predeformation direction (i.e., z direction), which is contrary to the creep process with an isotropic relaxation. The result is

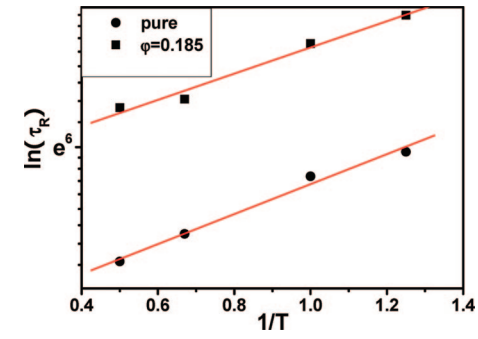

Figure 17. Logarithm of the conformational relaxation time τ_R as a function of the inverse of the temperature. The figure presents a good linear relationship between the logarithm of the relaxation time and the inverse of the temperature.

the same for the filled system. It may be because the polymer chains gradually return back to the coiled state from the elongated state during the conformational relaxation, and subsequently the chains slide between each other in order to maintain the fixed strain state in the z direction, which results in stronger mobility and more accelerated relaxation in the z direction.

4. Conclusions

On the basis of an idealized elastomer and nanoparticle model, we have systematically studied the structural and dynamic properties of nanofilled elastomer. Through the simulation, we observed that the introduced nanoparticles induce more efficient chain packing for attractive monomer/nanoparticle interaction. The calculated first layer content around the nanoparticle increases linearly with the filler loadings. By monitoring the

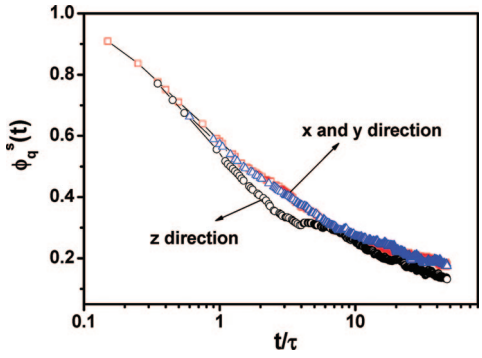

Figure 18. Incoherent intermediate dynamic structure factors $\phi_q^s(t)$ in the x, y, and z directions for the pure system during the relaxation process after the deformation in the z direction. τ is referred to the unit time of the simulation.

trajectory of a chosen monomer, we found the existence of a mobility gradient approaching the nanoparticle. For the dynamic properties, we found for the first time that both the time−concentration and time−temperature superposition principle(TCSP and TTSP) are applicable at the chain length scale for the terminal relaxation of the filled systems, while both break down at the segmental length scale. On the contrary, the TTSP holds at the segmental length scale for the pure system. Meanwhile, it was found that the logarithms of the characteristic relaxation time of the incoherent intermediate dynamic structure (IIDS) factor $\phi_q^s(t)$ and the end-to-end vector correlation $\phi_{ete}(t)$ scale linearly with the filler volume fraction. We conclude that the introduced nanoparticles have the similar effect on the polymer dynamics with thermodynamic properties such as the temperature and pressure.

Furthermore, we also studied the conformational relaxation process, indirectly reflecting the stress relaxation. The bond orientation during deformation and the decay of bond orientation during relaxation are studied by changing the draw ratio, the filler loadings, and the polymer/nanoparticle interaction. The value characterizing the bond orientation is higher at large draw ratio and high filler loadings with attractive nanoparticle/polymer interaction. By defining a variable characterizing the conformational relaxation, it is found that the conformational relaxation behavior can be approximately well fitted by an exponential or stretched exponential functions, similar to the stress relaxation. By fitting these curves, the obtained relaxation time increases with the increase of the filler loadings and the affinity between the nanoparticle and polymer. Importantly, we observe the time−temperature superposition principle almost holds for the conformational relaxation of the pure system, while breaks down for the filled system. The relaxation time of the conformational relaxation for the pure and filled systems exhibits an Arrhenius relationship with respect to the temperature. Finally, we studied the polymer dynamics during the relaxation. Contrary to the creep process, an anistropic dynamics was found with a slightly accelerated relaxation in the predeformed direction during the conformational or stress relaxation process. Remarkably, this work also presents that the time−temperature-concentration superposition principle (TTCSP) holds for the rheological properties of polymer nanocomposites with good nanoparticle dispersion (the filler network is not included here), which will provide new insights into the physical mechanisms governing the rheological properties of a wide range of polymer nanocomposites. Of course, the corresponding experiments are encouraged to give further support for this finding.

Acknowledgment. This work is supported by the National Natural Science Foundation of China (20776005, 20874005), the Outstanding Young Scientists Foundation of NSF of China (50725310), Beijing Novel Program (2006B17), the Programs for Important Project and New Century Excellent Talents (NCET-06-0095) from the Ministry of Education, and "Chemical Grid Project" and Excellent Talents Funding of BUCT.

References and Notes

(1) Tuteja, A.; Duxbury, P. M.; Mackay, M. E. *Phys. Rev. Lett.* **2008**, *1*, 077801.
(2) Mackay, M. E.; Tuteja, A.; Duxbury, P. M.; Hawker, C. J.; Van Horn, B.; Guan, Z. B.; Chen, G. H.; Krishnan, R. S. *Science* **2006**, *311*, 1740.
(3) Sen, S.; Xie, Y. P.; Kumar, S. K.; Yang, H. C.; Bansal, A.; Ho, D. L.; Hall, L.; Hooper, J. B.; Schweizer, K. S. *Phys. Rev. Lett.* **2007**, *98*, 128302.
(4) Mark, J. E.; Abou-Hussein, R.; Sen, T. Z.; Kloczkowski, A. *Polymer* **2005**, *46*, 8894.
(5) Kloczkowski, A.; Sharaf, M. A.; Mark, J. E. *Chem. Eng. Sci.* **1994**, *49*, 2889.
(6) Erguney, F. M.; Lin, H.; Mattice, W. L. *Polymer* **2006**, *47*, 3689.
(7) Lin, H.; Erguney, F.; Mattice, W. L. *Polymer* **2005**, *46*, 6154.
(8) Vacatello, M. *Macromolecules* **2001**, *34*, 1946.
(9) Vacatello, M. *Macromolecules* **2002**, *35*, 8191.
(10) Starr, F. W.; Schroder, T. B.; Glotzer, S. C. *Macromolecules* **2002**, *35*, 4481.
(11) Starr, F. W. Schroder, T. B.; Glotzer, S. C. *Phys. Rev. E* **2001**, *64*, 021802/1.
(12) Kotsilkova, R.; Fragiadakis, D.; Pissis, P. *J. Polym. Sci., Part B: Polym. Phys.* **2005**, *43*, 522.
(13) Fragiadakis, D.; Pissis, P. *J. Non-Cryst. Solids* **2007**, *353*, 4344.
(14) Ash, B. J.; Siegel, R. W.; Schadler, L. S. *J. Polym. Sci., Part B: Polym. Phys.* **2004**, *42*, 4371.
(15) Tsagaropoulos, G.; Eisenberg, A. *Macromolecules* **1995**, *28*, 6067.
(16) Cosgrove, T.; Roberts, C.; Garasanin, T.; Schmidt, R. G.; Gordon, G. V. *Langmuir* **2002**, *18*, 10080.
(17) Roberts, C.; Cosgrove, T.; Schmidt, R. G.; Gordon, G. V. *Macromolecules* **2001**, *34*, 538.
(18) Kalfus, J.; Jancar, J. *J. Polym. Sci., Part B: Polym. Phys.* **2007**, *45*, 1380.
(19) Gagliardi, S.; Arrighi, V.; Ferguson, R.; Telling, M. T. F. *Physica B* **2001**, *301*, 110.
(20) Kropka, J. M.; Putz, K. W.; Pryamitsyn, V.; Ganesan, V.; Green, P. F. *Macromolecules* **2007**, *40*, 5424.
(21) Kropka, J. M.; Sakai, V. G.; Green, P. F. *Nano Lett.* **2008**, *8*, 1061.
(22) Montes, H.; Lequeux, F.; Berriot, J. *Macromolecules* **2003**, *36*, 8107.
(23) Berriot, J.; Montes, H.; Lequeux, F.; Long, D.; Sotta, P. *Macromolecules* **2002**, *35*, 9756.
(24) Bogoslovov, R. B.; Roland, C. M.; Ellis, A. R.; Randall, A. M.; Robertson, C. G. *Macromolecules* **2008**, *41*, 1289.
(25) Tuteja, A.; Mackay, M. E.; Hawker, C. J.; Van Horn, B. *Macromolecules* **2005**, *38*, 8000.
(26) Mackay, M. E.; Dao, T. T.; Tuteja, A.; Ho, D. L.; Van Horn, B.; Kim, H. C.; Hawker, C. J. *Nat. Mater.* **2003**, *2*, 762.
(27) Cosgrove, T.; Roberts, C.; Choi, Y.; Schmidt, R. G.; Gordon, G. V.; Goodwin, A. J.; Kretschmer, A. *Langmuir* **2002**, *18*, 10075.
(28) Sternstein, S. S.; Zhu, A. J. *Macromolecules* **2002**, *35*, 7262.
(29) Thomin, J. D.; Keblinski, P.; Kmnar, S. K. *Macromolecules* **2008**, *41*, 5988.
(30) Sen, S.; Thomin, J. D.; Kumar, S. K.; Keblinski, P. *Macromolecules* **2007**, *40*, 4059.
(31) Heinrich, G.; Kluppel, M. *Filled Elastomers Drug Delivery Systems*; Springer-Verlag Berlin: Berlin, 2002; Vol. 160, p 1.
(32) Kluppel, M. *Filler-Reinforced Elastomers Scanning Force Microscopy*; Springer-Verlag Berlin: Berlin, 2003; Vol. 164, p 1.
(33) Heinrich, G.; Kluppel, M.; Vilgis, T. A. *Curr. Opin. Solid State Mat. Sci.* **2002**, *6*, 195.
(34) Bokobza, L. *Macromol. Mater. Eng.* **2004**, *289*, 607.
(35) Wang, M. J.; Lu, S. X.; Mahmud, K. *J. Polym. Sci., Part B: Polym. Phys.* **2000**, *38*, 1240.
(36) Madkour, T M. In *Polymer Data Handbook*; Mark, J. E., Ed.; Oxford University Press: New York, 1999.
(37) Ronan, S.; Alshuth, T.; Jerrams, S.; Murphy, N. *Mater. Design* **2007**, *28*, 1513.
(38) Madkour, T. M. *J. Appl. Polym. Sci.* **2004**, *92*, 3387.
(39) Gao, J.; Weiner, J. H. *J. Chem. Phys.* **1995**, *103*, 1614.
(40) Gao, J.; Weiner, J. H. *J. Chem. Phys.* **1995**, *103*, 1621.
(41) Loriot, G.; Weiner, J. H. *J. Polym. Sci., Part B: Polym. Phys.* **1998**, *36*, 143.
(42) Gao, J.; Weiner, J. H. *J. Chem. Phys.* **1992**, *97*, 8698.
(43) Gao, J.; Weiner, J. H. *Macromolecules* **1994**, *27*, 1201.
(44) Gao, J. P.; Weiner, J. H. *Science* **1994**, *266*, 748.
(45) Gao, J. P.; Weiner, J. H. *Macromolecules* **1996**, *29*, 6048.

(46) Harmandaris, V. A.; Mavrantzas, V. G.; Theodorou, D. N. *Macromolecules* **2000**, *33*, 8062.
(47) Zeng, Q. H.; Yu, A. B.; Lu, G. Q. *Prog. Polym. Sci.* **2008**, *33*, 191.
(48) Allegra, G.; Raos, G.; Vacatello, M. *Prog. Polym. Sci.* **2008**, *33*, 683.
(49) Bower, A. F.; Weiner, J. H. *J. Chem. Phys.* **2006**, *125*, 096101.
(50) Bower, A. F.; Weiner, J. H. *J. Chem. Phys.* **2004**, *120*, 11948.
(51) Liu, J.; Wu, S. Z.; Cao, D. P.; Zhang, L. Q. *J. Chem. Phys.* **2008**, *129*, 154905.
(52) Liu, J.; Cao, D. P.; Zhang, L. Q. *J. Phys. Chem. C* **2008**, *112*, 6653.
(53) Allen, M. P.; Tildesley, D. J. *Computer Simulation of Liquids*; Oxford University Press: Oxford, U.K., 1987.
(54) Plimpton, S. J. *J. Comput. Phys* **1995**, *117*, 1.
(55) Ni, R.; Cao, D. P.; Wang, W. C.; Jusufi, A. *Macromolecules* **2008**, *41*, 5477.
(56) Abrams, C. F.; Kremer, K. *J. Chem. Phys.* **2001**, *115*, 2776.
(57) Dodd, L. R.; Theodorou, D. N. *Mol. Phys.* **1991**, *72*, 1313.
(58) Picu, R. C.; Ozmusul, M. S. *J. Chem. Phys.* **2003**, *118*, 11239.
(59) Elzein, T.; Galliano, A.; Bistac, S. *J. Polym. Sci., Part B: Polym. Phys.* **2004**, *42*, 2348.
(60) Hooper, J. B.; Schweizer, K. S. *Macromolecules* **2005**, *38*, 8858.
(61) Dionne, P. J.; Picu, C. R.; Ozisik, R. *Macromolecules* **2006**, *39*, 3089.
(62) Bharadwaj, R. K.; Boyd, R. H. *Macromolecules* **2000**, *33*, 5897.
(63) Donnet, J. B.; Vidal, A. *Adv. Polym. Sci.* **1986**, *76*, 103.
(64) Heymans, N. *Signal Process.* **2003**, *83*, 2345.
(65) Hua, C. C.; Wu, M. S. *J. Polym. Sci., Part B: Polym. Phys.* **2006**, *44*, 787.
(66) Gestoso, P.; Brisson, J. *J. Polym. Sci., Part B: Polym. Phys.* **2002**, *40*, 1601.
(67) Duchesne, C. E. *Thesis.* Universite Laval: Quebec, Canada, 1999.
(68) Li, D.; Brisson, J. *Polymer* **1994**, *35*, 2078.
(69) Riggleman, R. A.; Schweizer, K. S.; de Pablo, J. J. *Macromolecules* **2008**, *41*, 4969.

MA802744E